

Super-solar N/C in the NLS1 Galaxy Markarian 1044

Dale L. Fields¹, Smita Mathur¹, Richard W. Pogge¹, Fabrizio Nicastro² & Stefanie Komossa³

fields@astronomy.ohio-state.edu

ABSTRACT

Narrow-Line Seyfert 1s (NLS1s) are known to have extreme values of a number of properties compared to Active Galactic Nuclei (AGN) as a class. In particular, previous emission-line studies have suggested that NLS1s are unusually metal rich compared to broad-line AGN of comparable luminosity. We present low- and medium-resolution spectroscopic observations of the NLS1 Markarian 1044 with the Hubble Space Telescope Imaging Spectrometer (STIS). We identify two blueshifted intrinsic absorption systems at -1145 and -295 km s^{-1} relative to the systemic velocity of the galaxy. Using a simple photoionization model of the absorbing gas, we find that the strongest and best-measured of the absorption systems has $N/C \approx 6.96 [N/C]_{\odot}$. We also report on the discovery of three new Ly α forest lines with $\log N_{HI} \geq 12.77$. This number is consistent with the 2.6 expected in the path length to the source redshift of Mrk 1044.

1. Introduction

The Narrow-Line Seyfert 1 (NLS1) class has come a long way since being identified by Osterbrock & Pogge (1985). There, they were defined as Seyfert 1s with relatively narrow permitted lines ($\leq 2000 \text{ km s}^{-1}$) and a weak [O III]/H β ratio (≤ 3). The principal component analysis of Boroson & Green (1992) found that NLS1s lie at one extreme end of the eigenvector with the most variation in AGN spectral properties. In addition, NLS1s often have very steep X-ray spectra, placing them on one end of the anti-correlation between soft X-ray spectral slope and H β FWHM seen in Seyfert 1s (Boller, Brandt & Fink 1996) and quasars (Laor et al. 1997).

¹Department of Astronomy, the Ohio State University, 140 West 18th Avenue, Columbus, OH 43210, USA

²SAO, 60 Garden Street, 02138, Cambridge, MA, USA

³Max-Planck-Institut für extraterrestrische Physik, Giessenbachstrasse 1, D-85748 Garching, Germany

While work continues to identify the physical driver of eigenvector 1, the leading contender is accretion rate expressed as a fraction of the Eddington accretion rate ($\dot{m} = \dot{M}/\dot{M}_{\text{Edd}}$) as suggested by Pounds, Done & Osborne (1995). This would imply that NLS1s and some quasars are accreting at a large fraction of the Eddington rate. This receives support from evidence that NLS1s appear to have smaller supermassive black holes than many other Seyferts, and yet have comparable luminosities (Grupe et al. 2004, and references therein) and references therein. Another type of AGN suspected to have a large fractional accretion rate are the high-redshift quasars. These have much larger luminosities, and correspondingly larger black hole masses than other AGN.

One other property that NLS1s and high-redshift quasars appear to share is super-solar gas-phase metallicity. The NLS1 PG1404+226 has unusually strong N V absorption lines relative to Ly α , C IV and X-ray absorption features, and this can only be explained by super-solar metallicity (Mathur 2000b). Wills et al. (1999) found that the strengths of the N V λ 1240 emission lines systematically stronger than average, and the C IV λ 1549 were systematically weaker in AGN with narrow permitted lines. This is similar to what appears in high redshift quasars (Hamann & Ferland 1999; Osmer et al. 1994; Shields & Hamann 1997). In addition, the strength of the fluorescent Fe-K α emission line in some NLS1s is also thought to indicate super-solar abundances (Collin & Joly 2000). Finally, Komossa & Mathur (2001) noted that the steep X-ray spectra seen in NLS1s eliminates the possibility of having a multi-phase medium with solar abundances. Only if the gas is super-solar can it successfully form a pressure-confined broad-line region.

Metallicity, and more importantly, abundance ratios reflect the star formation history of the nuclear gas. This in turn might tell us about the particular circumstances leading to the activation of the AGN. There are theories that link the many similarities between NLS1s and quasars into a scenario stating that these objects are “young,” that is, the black holes have recently begun (re-)accreting gas (Mathur 2000a). In the case of Narrow-Line Seyfert 1s, this is very likely, as the mass e-folding time is short enough to conclude that if that black hole had any similarly major accretion events in its past, it would not have the relatively low mass it has today. There are even suggestions that some NLS1s do not fall directly on the $M_{BH} - \sigma$ relation (Mathur et al. 2001; Grupe & Mathur 2004). Because NLS1s could be part of an evolutionary track (as opposed to the Unified Model), there is no a priori reason why NLS1s should have the same star formation history, and thus metal abundance ratios, as normal Seyfert galaxies. Indeed, Shemmer & Netzer (2002) find that NLS1s have significantly higher N V/C IV ratios than standard Seyferts. This result, however, is not confirmed in N IV/C IV. In addition, data on this ratio is based upon emission line ratios. A single emission line can originate in multiple locations, each with different physical conditions, complicating the conversion of line flux to column densities to abundance. If one wishes to

get an unambiguous result, one has to measure the absorption lines. With this in mind, the emission lines results indicate super-solar metallicity (Hamann & Ferland 1999), but require confirmation.

We seek to determine the metal abundance of a NLS1 using absorption lines. The largest contributor to the uncertainty in the abundances is the uncertainty in the photoionization correction. This must be well determined if there is to be any confidence in our results. Historically, studies have contained few transitions and few (sometimes only one) species per element due to limited wavelength coverage (e.g. only UV or only X-ray) and thus do not have the leverage to determine the correct ionization model. Our program consists of near-simultaneous observations of the NLS1 Markarian 1044 with the HST, FUSE, and Chandra observatories. This long wavelength baseline ensures that we will have the range of species and elements to accurately model the ionization correction. In this paper, we present observations of Mrk 1044 with the FUV-MAMA instrument onboard the Hubble Space Telescope. Future papers will detail the FUSE and Chandra observations and the self-consistent model derived from all three’s observations. In §2 we detail the the FUV-MAMA observation and data. We then follow in §3 with the analysis. We discuss the results in §4 and give concluding remarks in §5.

2. Observations and Data Reduction

Mrk 1044 was observed on UTC 2003 Jun 28 using the Hubble Space Telescope Imaging Spectrometer (STIS) with the FUV-MAMA detector. All observations were acquired during a single 5-orbit visit that ran from MJD 52818.19912 through MJD 52818.49349. A journal of observations is given in Table 1. The 52X0.2 aperture and a clear filter were used for all observations, centering the aperture on the bright nucleus of Mrk 1044. Two low-dispersion UV spectra with the G140L grating (central wavelength of $\lambda 1426\text{\AA}$) were acquired during the first orbit, with a cumulative exposure time of 2311 seconds. Medium-dispersion spectra were acquired with the G140M grating during the remaining 4 orbits at central wavelengths of $\lambda 1222$, $\lambda 1272$, and $\lambda 1567$ covering the emission lines of Ly α , N V, and C IV, respectively. The Ly α and C IV regions were observed for 1 orbit each, acquiring 2 spectra per orbit for cumulative exposure times of 2734 seconds each, and N V was observed for 2 orbits (4 spectra) for a cumulative exposure time of 5583 seconds.

The standard STSDAS¹ `calstis` pipeline was used to reduce the raw data to wavelength- and flux-calibrated 2D spectra. The nuclear spectra of Mrk 1044 were extracted from the

¹STSDAS is a product of the Space Telescope Science Institute, which is operated by AURA for NASA.

linearized 2D spectra (STIS “x2d” science frames) using a 9 pixel (0.45 arcsec) aperture using the `spectroid` centroiding aperture-extraction task in XVista². Corresponding error spectra were also extracted from the STIS error arrays for each spectrum and co-added in quadrature. These 1D spectra form the basis of our subsequent analysis.

The G140L spectrum provides us with a reliable internal relative intensity calibration for the three non-overlapping G140M spectra, and provides information on the overall UV spectral slope. The G140L spectrum with the flux-calibrated G140M spectra superimposed is shown in Figure 1. The individual flux-calibrated G140M spectra are shown in Figure 2.

3. Analysis

As can be seen in Figure 1, the UV spectrum of Mrk 1044 has a flat UV continuum with a slope of $\alpha = 0.0$ for $f_\nu \propto \nu^{-\alpha}$. Its emission line features are similar to those of many other AGN. Most prominent are the Ly α , N V, and C IV emission lines. Less prominent, but certainly present are the Si II λ 1265, O I λ 1305, C II λ 1335, Si IV λ 1394,1403+O IV] λ 1402, N IV] λ 1486, He II λ 1640, and O III] λ 1663 lines. Emission lines in general have a narrow ($< 1500 \text{ km s}^{-1}$) component and a broad ($> 3000 \text{ km s}^{-1}$) base. The presence of this base causes significant blending of Ly α and N V.

The three G140M spectra show a total of 26 possible absorption lines, all but four of which have good identifications. Line identification proceeded from three assumptions: 1) lines near the rest-frame wavelength of a well-known and strong transition are likely due to Galactic ISM, 2) any N V or C IV absorption line systems intrinsic to Mrk 1044 will also appear at the same velocity in Ly α , and 3) any remaining unidentified absorption lines blueward of Mrk 1044’s Ly α emission line, but redward of 1216Å could be the signature of the low redshift Ly α forest.

Line doublets of N V and C IV were identified by superposing velocity maps for each of the doublets. From the NASA/IPAC Extragalactic Database (NED), we adopt a systemic velocity of Mrk 1044 of 4932 km s^{-1} ($z=0.01645$). Velocity maps are shown in Figure 3 for Ly α , N V, and C IV. From these, we identify two absorption systems at -1145 km s^{-1} and -295 km s^{-1} . We find that the two candidate absorption systems in N V at -2100 km s^{-1} and $+75 \text{ km s}^{-1}$ are actually Galactic absorption from S II λ 1251,1254 in the case of the former and S II λ 1260 and an unknown absorption line superposed in velocity space in the

²XVista is the current incarnation of Lick Observatory Vista, maintained in the public domain at <http://ganymede.nmsu.edu/holtz/xvista>.

case of the latter. In both cases, no corresponding absorption system is detected in C IV or in Ly α .

We use two methods (each with slightly varying analysis paths) to measure the column densities of the absorbing material. The first is the standard curve of growth. More details of this process may be found in Spitzer (1978). To determine the velocity spread parameter, we calculate values of the column density for each line for 'b' values of 10, 20, 40, and 80 km s⁻¹. We then assume the velocity spread that gives the most consistent result between the line pair. The second method is the apparent optical depth method described by Savage & Sembach (1991). This method is usable in well-resolved systems and thus it will provide an independent method with which to estimate the column densities.

Lines in each of the spectra were first measured approximately with the analysis package LINER (Pogge & Owen 1993). Best fit parameters for the emission lines were then used as initial guesses into the STSDAS analysis package SPECFIT (Kriss 1994). To determine the absorption line parameters via the curve of growth method, LINER was used with a local continuum parameterized by fitting a fifth order polynomial over a limited wavelength range (e.g. only on one side of an emission line). A polynomial of order five was found to be a good balance between fitting the intrinsic structure of the continuum and letting noise introduce unphysical structure into the continuum fitting. In this manner, the local continuum and then two or three absorption lines would be fit and the process repeated for the next absorption feature. Again, these results were used as inputs into SPECFIT for final determination of the equivalent widths.

The analysis of the lines using the apparent optical depth method proceeded differently. Because estimating the continuum is the single largest contributor to the systematic error budget, we performed nine by-eye spline fits to the continuum around each group of lines. All nine were done as reasonable fits, but several were purposefully fit to the outer envelope of the noise. A mean was then taken of the nine resultant column densities with the scatter functioning as our measurement of error.

3.1. Mrk 1044 Emission Lines

Most of the metallicity studies of AGN have been restricted to using the emission lines only. Therefore, we give measurements of our emission lines to place the results of our absorption line study within the proper context. For each ion Table 2 gives the rest wavelength, the observed equivalent width, and the FWHM of the fit components. For most emission lines we fit both a narrow and a broad component. Both the N V and C IV emission lines

exhibited an excess of red-ward flux which we parameterized with an additional Gaussian. The Si IV+O IV] complex around 1400Å can be parameterized with several narrow components and one very broad one, but these are so poorly constrained individually that we only report the gross properties of the complex.

The literature contains many measures of AGN metallicity. Shemmer & Netzer (2002)’s Figure 2 gives N V/C IV and N V/He II as a function of νL_ν at 1450Å. Mrk 1044 has ratios of 0.6 and 3.1, respectively, at $1.3 \times 10^{12} L_\odot$. These values place Mrk 1044 right in the middle of the NLS1 metallicity distributions, though this object is slightly more luminous than the rest of the NLS1 sample considered by Shemmer & Netzer (2002). Nevertheless, Mrk 1044 remains at or above the mean metallicity-luminosity correlation. We can also place Mrk 1044 alongside the ultraviolet measurements of NLS1s in Wills et al. (2000). This object’s C IV/Ly α value of 0.59 is slightly higher than any of the NLS1s shown in their Figure 2. Mrk 1044’s (Si IV+O IV)]/Ly α value of 0.17 is at the upper value bounded by their NLS1 sample. Finally, we can compare this object against the “nitrogen-rich” quasar Q0353-383 (Osmer 1980) and its recently discovered fraternity (Bentz & Osmer 2004). One of the metallicity indicator used in these studies is $f_{CIV}/(f_{Ly\alpha} + f_{NV})$, of which Q0353-383 has the lowest value found to date: 0.07. By comparison, Mrk 1044 has a value of 0.45, a factor of six difference. It should be noted that (Osmer 1980) found a value of $N/C \approx 10\text{-}20 [N/C]_\odot$, which is only a factor of 2-3 higher than the value we will discuss below in §4.

3.2. Mrk 1044 Absorption Line Systems

Of the 24 absorption lines found in our UV spectra, 10 of these appear to be intrinsic to Mrk 1044, organized into two distinct absorption systems. System 1 at -1145 km s^{-1} contains strong lines of Ly α , N V, and C IV. System 2 at -295 km s^{-1} contains strong lines of Ly α and C IV, but has weak N V. Due to their inherent weakness, estimations of the strengths of the N V lines in System 2 suffer accordingly. Table 3 gives the measured and derived parameters for these systems: the observed wavelength, the observed equivalent width, the column densities derived both the curve of growth method and the optical depth integration, and the velocity offset from the systemic. Equivalent widths are typically around 0.2Å in the case of System 1 and 0.02Å in the case of System 2. The errors in the equivalent widths were determined by using estimates of the photon noise in each pixel. The errors in the velocity are set at 0.5 pixels, as given by the STIS Instrument Handbook for Cycle 13. Centroiding errors are much smaller and therefore ignored.

When we calculate the column densities using the curve of growth method, we find that a velocity spread parameter of 20 km s^{-1} gives the most consistent result for both pairs of

N V and C IV lines. If we assume that this contributes the greatest to the width of the line, we can determine if these lines are fully resolved. The STIS Instrument Handbook gives a nominal spectral resolution of 1.4 pixels. This corresponds to between 18 and 14 km s^{-1} in width at the lines of N V and C IV, respectively. This is approximately similar to the preferred curve of growth width of 20 km s^{-1} so we will use that as our measure of intrinsic width. In the case of System 1, the FWHM of the N V and C IV line pairs are 71, 71, 50 and 47 km s^{-1} , from blue to red. All of these lines are fully resolved. In the case of System 2, the FWHM of the lines are 90, 100, 43 and 38 km s^{-1} . The C IV lines are close to being resolved. While the best-fit values of the N V line widths suggest these two lines are resolved, the large uncertainties prevent this from being definite.

We calculate the degree of saturation of these two systems by measuring the ratios of the equivalent widths of each line doublet. Both N V and C IV have natural ratios of 2.0. This can be used to derive a covering fraction (C_f) for each system following Hamann et al. (1997). System 1 has a consistent value of $C_f = 0.80$ determined from both the N V and C IV lines. System 2 has less consistent values with C_f of 0.97 (N V) and 0.94 (C IV), but this is not unexpected given the more marginal nature of System 2’s N V doublet, the $\lambda 1243\text{\AA}$ line of which we only detect at about the 2.5σ level.

We calculate N V/C IV column ratios for Systems 1 and 2. We use the weighted mean for each species from each doublet. As Table 3 shows, both methods find very similar results for the N V abundance, but the curve of growth method finds a systematically smaller C IV abundance than the apparent optical depth method. This does not affect the N V/C IV column ratios at the 3σ level. In System 1, we find N V/C IV ratios of $2.7 \pm 7\%$ and $2.0 \pm 10\%$ for the curve-of-growth and optical depth methods, respectively. For System 2 we find ratios of $1.0 \pm 20\%$ and $0.7 \pm 30\%$ for the two methods respectively.

3.3. Galactic Absorption Lines

With good certainty, we detect absorption lines of N I, $\text{Ly}\alpha$, Si II, Si III, S II, and C IV in our medium-resolution spectra and $\text{Ly}\alpha$, O I, C II, and Si II in our low-resolution spectrum from the ISM of our galaxy. To determine the velocity spread parameter b for the curve of growth method, we look for the most consistent result between lines of the same species. Species for which we have only a single identified line we report a range of densities corresponding to a range of b of 20-80 km s^{-1} . We also report column densities using the apparent optical depth method for all lines. We give the results in Table 4 in the form of observed wavelength, likely identification, the candidate’s rest wavelength, the velocity width, the observed equivalent width, the derived column densities for both methods, and

the velocity relative to Mrk1044’s systematic velocity. The velocities of the absorption components are scattered about zero and, in 12 of 14 cases, within three standard deviations of zero. It should be noted that there are systematic velocity shifts with respect to the parent spectrum. Two of the G140M spectra (Ly α and C IV) have all their Galactic absorption lines shifted to the blue, while the other G140M spectrum (N V) and the G140L spectrum have their Galactic absorption lines shifted to the red. This can also be seen, though not as clearly, in the lines given in Table 3. These shifts are not statistically significant if one accepts the absolute wavelength calibration error of 0.5 pixels. The errors in the equivalent widths are estimated from the photon noise.

Most of the FWHMs of the lines in the medium-resolution spectra sit between 50 and 70 km s⁻¹ with a few lines $\gtrsim 100$ km s⁻¹ (the Si lines and C IV λ 1548). The uncertainty in the width is not taken from any SPECFIT fit (which claims a formal precision on the order of one-tenth to one percent error on any one measurement) but instead from the scatter around the mean width measurement over many continuum fittings. This uncertainty is approximately 5 km s⁻¹ for almost all lines. The S II triplet lines have the best agreement amongst themselves, all coming within one standard deviation of their mean width, 61 km s⁻¹. The N I lines have a mean width of 70 km s⁻¹ and agree to within one standard deviation. The Si lines have a mean width of 126 km s⁻¹ and agree to within one standard deviation. The only real disagreement is from the C IV lines which disagree at greater than three standard deviations.

The Galactic C IV lines suffer from another problem. The velocities (i.e. centroids) of these lines are in great disagreement with each other. The uncertainty in the velocity given is that induced by the absolute wavelength calibration. Wavelengths relative to one another in the same spectrum have their uncertainties smaller by a factor of 2.5 to 5. This creates a disagreement in the centroids of the C IV lines of more than 6σ . In addition, as can be seen from visual inspection of the spectrum (Figure 2), the profiles of these lines are dissimilar. It is possible that weak absorption from High Velocity Clouds (HVCs) is preferentially altering the shape of the stronger C IV λ 1548 line. This could also explain the large differences in the FWHM of these lines. This hypothesis, however, cannot be tested with the current data and must wait for FUSE confirmations of the existence of HVCs through the detection (or not) of O VI.

The three absorption lines in the G140L spectrum (O I, C II, and Si II λ 1527) have large widths of 920, 560, and 390 km s⁻¹, respectively. All are fully resolved. It is possible that what we identify as simply O I could also be blended with S I λ 1303. This would explain the large width and would eliminate O I’s large inferred velocity. Unfortunately, deblending does not return a clean result, so we cannot make this correction with any certainty and instead

elect to omit it. The large values of inferred widths in the G140L spectrum is somewhat surprising, given that the low ionization lines seen in the higher resolution spectra are all so narrow. The cause of this is not yet known and we caution anyone from trusting the properties of these lines at this time.

The four unidentified absorption lines fail at least one of our criteria. To be identified, a line must come from a strong transition of an abundant element without having a sufficiently large velocity difference. For example, Si II $\lambda 1264.7\text{\AA}$ could be identified with the line at 1263.5\AA but for the fact that this would give it a relative velocity of -286 km s^{-1} . We also use additional information such as the fact that the line in question has a width of 52 km s^{-1} which makes it unlikely to come from Si whose lines average 123 km s^{-1} . It is possible that the absorption lines near the Ly α emission line of Mrk 1044 are Ly α whose systems simply do not have the column to appear in N V or C IV.

3.4. Intervening Ly α Absorption?

The two unidentified absorption lines blueward of the Ly α emission line have velocities relative to Mrk 1044's systemic velocity of about 2000 and 3000 km s^{-1} . While this does not particularly favor an origin as material intrinsic to Mrk 1044, it is not inconsistent with that hypothesis. If these absorption lines are due to intrinsic Ly α , the inferred column densities are intermediate between Systems 1 and 2. Unlike those two systems, however, these unidentified systems do not show absorption in either N V or C IV. An alternative hypothesis is that these two systems are due to the low-redshift Ly α -forest. To test this, we calculate the number of expected absorption systems from the results of Penton et al. (2004). They parameterize the number of systems per unit log column density and per unit redshift $\partial^2 N / \partial N_{HI} \partial z$ as $C_{HI} N_{HI}^{-\beta}$ with $C_{HI} = 10^{10.3}$ and $\beta = 1.65$ between $\log N_{HI}$ of 12.3 and 14.5. We calculate the 3σ detection limit of Ly α absorption to be $\log N_{HI} = 12.77$. Because this is almost a factor of ten lower in column density than the weaker of our systems, we reanalyze the spectrum for weak lines. Our best continuum fit (flattest continuum-divided spectrum) can be seen in Figure 4. While any one continuum fit may produce several well-detected line candidates, we require any line to be well-detected in the majority of our nine continuum fits. Only one additional line passes this test, being detected, on average, at exactly 3σ . The wavelengths, velocity widths, equivalent widths, calculated column densities and relative velocities of the two strong Ly α systems and the weak, newly found system are given in Table 5. For the decade above our detection limit, and for a path length $\Delta z = z_{\text{Mrk 1044}} = 0.01645$, 2.0 systems are expected, and two systems (within our column density errors) are detected. The expected number of systems at all higher column densities

($\log N_{HI} > 13.77$) and the same path length is 0.6 and we detect one. In this manner, the attribution of these absorption lines to intergalactic Ly α absorption is perfectly reasonable.

4. Discussion

The N V/C IV ratio does not tell us the N/C abundance ratio until we apply an ionization correction for each species. This ionization correction is the greatest source of systematic uncertainty in the determination of abundances. An accurate ionization correction requires measurements of multiple species of a single element, and preferably as many additional elements as possible. For this reason, we cannot create an accurate ionization model with just this HST data. We are able, however, to set a lower limit on the N/C abundance ratio by calculating the N V/C IV ratio in a region with physical parameters optimized such that the maximum amount of N is in N V. We invert the equation

$$\frac{N\ V}{C\ IV} = \frac{A(N)}{A(C)} \times \frac{(N\ V/N)}{(C\ IV/C)} \quad (1)$$

where $A(N)/A(C)$ is the total Nitrogen to total Carbon abundance ratio (henceforth N/C), the quantity we want to measure. Following Hamann & Ferland (1999) (their Figure 10), we find that N V has a maximum ionization fraction of 0.40 at $\log U$ of -1.55 . The fraction of carbon in C IV at the same ionization parameter is 0.31. Using our observed ratio of $N\ V/C\ IV=2.67$ from System 1, this gives a N/C ratio of 2.07, or $6.96 [N/C]_{\odot}$ ($\pm 7\%$). Doing the same analysis with the weaker absorption lines of System 2 gives a super-solar N/C ratio of only $2.3 [N/C]_{\odot}$ ($\pm 20\%$). The errors quoted only incorporate uncertainties due to measurements derived from the spectra.

To demonstrate the discrepancies caused by improper ionization corrections, we compute N/C for two alternative models. We do this by running the photoionization-equilibrium code Cloudy 94³ (Ferland et al. 1998) with two differing spectral energy distributions (SEDs): a power law SED with $\alpha = -1.5$ and Cloudy’s standard AGN SED. We find that System 1 has an abundance ratio of $4.3 [N/C]_{\odot}$ in the case of the simple power law SED and $2.9 [N/C]_{\odot}$ in the case of the standard AGN template SED. This can be compared with value of 6.96 using Hamann & Ferland (1999) as above. The estimated error due to photon noise is only $\sim 7\%$, which demonstrates that our result is dominated by systematic uncertainty in the ionization corrections, and more accurate results await data at other wavebands that should

³Cloudy version C94.00, obtained from the Cloudy webpage <http://www.nublado.org/>

permit calculation of a detailed photoionization model for these spectra. Until such a model is constructed, we are limited to stating only that Mrk 1044 has line strengths consistent with a super-solar N/C ratio.

5. Conclusions

We have analyzed FUV-MAMA spectra of the Narrow-Line Seyfert 1 galaxy Mrk 1044. We find two absorption systems blueshifted with respect to the systemic velocity of the galaxy. We find absorption lines from Galactic ISM in both the low-resolution and medium-resolution spectra. We find super-solar N/C in the outflow systems of Mrk 1044 utilizing a very simple ionization model. We defer constructing a more detailed photoionization model until after analyzing the FUSE and Chandra data so as to avoid the problems that have historically plagued models derived from single wavelength regions.

The authors wish to thank Mike Crenshaw for his assistance with the apparent optical depth method. This research has made use of the NASA/IPAC Extragalactic Database (NED) which is operated by the Jet Propulsion Laboratory, California Institute of Technology, under contract with the National Aeronautics and Space Administration. Primary support for this work was provided by NASA grant HST-GO-09687.O2 from the Space Telescope Science Institute, which is operated by the Association of Universities for Research in Astronomy, Inc., under NASA contract NAS 5-26555.

REFERENCES

- Bentz, M. & Osmer, P. 2004, *AJ*, 127, 576
- Boller, Th., Brandt, N., & Fink, H. 1996, *A&A*, 305, 53
- Boroson, T. & Green, R. 1992, *ApJS*, 80, 109
- Brandt, N. & Boller, Th. 1998, *A&A*, 319, 7
- Collin, S. & Joly, M. 2000 *New A Rev.*, 44, 531
- Ferland, G. J., Korista, K. T., Verner, D. A., Ferguson, J. W., Kingdon, J. B., Verner, E. M. 1998, *PASP*, 110, 761.
- Grupe, D. & Mathur, S. 2004, *ApJ*, 606L, 41

- Grupe, D., Wills, B.J., Leighly, K.M., & Meusinger, H. 2004 *AJ*, 127, 156
- Hamann, F., Barlow, T.A., Junkkarinen, V., Burbidge, E.M. 1997, *ApJ*, 478, 80
- Hamann, F. & Ferland, G. 1991, *ARA&A*, 37, 487
- Komossa, S. & Mathur, S. 2001, *A&A*, 974, 914
- Kriss, G.A. 1994 in *Astronomical Data Analysis Software & Systems III*, A.S.P. Conf. Series, Vol. 61, ed. D. R. Crabtree, R. J. Hanisch, & J. Barnes (Astronomical Society of the Pacific: San Francisco), p. 437.
- Laor, A., Fiore, F., Elvis, M., Wilkes, B., McDowell, J. 1997, *ApJ*, 477, 93
- Mathur, S. 2000, *MNRAS*, 314, L17
- Mathur, S. 2000, *New Astronomy Reviews*, 44, 469
- Mathur, S., Matt, G., Green, P.J., Elvis, M., Singh, K.P. 2001, *ApJ*, 551L, 13
- Osmer, P., Porter, A., Green, R. 1994, *ApJ*, 436, 678
- Osmer, P. 1980, *ApJ*, 237, 666
- Osterbrock, D.E. & Pogge, R.W. 1985, *ApJ*, 297, 166
- Penton, S.V., Stocke, J.T., & Shull, J.M. 2004, *ApJS*, 152, 29
- Pogge, R.W., & Owen, J.M. 1993, *LINER; An Interactive Spectral Line Analysis Program*, OSU Internal Report 93-01
- Pounds, K., Done, C., & Osborne, J. 1995, *MNRAS*, 277, L5
- Savage, B.D., & Sembach, K.R. 1991, *ApJ*, 379, 245
- Shemmer, O. & Netzer, H. 2002, *ApJ*, 567, L22
- Shields, J. & Hamann, F. 1997, *RMxAC*, 6, 221
- Spitzer, L. 1987, *Physical Processes in the Interstellar Medium* (New York: Wiley-Interscience), 46
- Wills, B. et al. 1999 in “Quasars and Cosmology”, Ed. G. Ferland & J. Baldwin
- Wills, B.J., Shang, Z. & Yuan, J.M. 2000, *New A Rev.*, 44, 511

Table 1. Journal of Observations

Grating	Central Wavelength [\AA]	UTC Date (start)	Exposure Times [s]	Datasets
G140L	1425	2003-06-28T04:46:49	1200 & 1011	O8K401010-20
G140M	1567	2003-06-28T06:14:08	1294 & 1440	O8K040130-40
	1222	2003-06-28T07:50:11	1294 & 1440	O8K040150-60
	1272	2003-06-28T09:26:15	1294, 1409 & 2×1440	O8K040170-a0

Table 2. Emission Lines

Ion	λ_{Rest} [\AA]	Equivalent Width [\AA]	FWHM-Narrow [km s^{-1}]	FWHM-Broad [km s^{-1}]
H I	1216	113.6 ± 0.1	1120.6 ± 0.3	3406 ± 3
N V	1239,1243	40.2 ± 0.4	1070 ± 40	5530 ± 50^a
O I	1302	4.9 ± 0.7	1350 ± 7	3600 ± 200
C II	1336	2.94 ± 0.04	1020 ± 20	3110 ± 50
Si IV+O IV]	1394,1403+1402	19.19 ± 0.03	~ 2000	~ 10000
N IV]	1486	0.984 ± 0.005	1262 ± 4	\dots
C IV	1548,1551	67.0 ± 0.3	1317 ± 3	3400 ± 30^b
He II	1640	12.9 ± 0.5	1440 ± 50	7500 ± 200
O III]	1663	5.2 ± 0.4	\dots	3400 ± 200

^aLine asymmetry requires a third (red) Gaussian with a width of 3450 ± 20

^bLine asymmetry requires a third (red) Gaussian with a width of 7320 ± 30

Table 3. Measured and Calculated Parameters of Mrk 1044

Line	Observed Wavelength [\AA]	FWHM [km s^{-1}]	Equivalent Width [m\AA]	$\log(\text{Column})$ [cm^{-2}] ^a	$\log(\text{Column})$ [cm^{-2}] ^b	Velocity [km s^{-1}]
System 1						
$\text{Ly}\alpha$	1230.9819	92 ± 7	341 ± 5	$15.07^{+0.05}_{-0.05}$	$14.11^{+0.04}_{-0.04}$	-1156 ± 7
N V1239	1254.4633	71 ± 3	209 ± 8	$14.38^{+0.05}_{-0.04}$	$14.33^{+0.03}_{-0.03}$	-1143 ± 6
N V1243	1258.4999	71 ± 3	162 ± 6	$14.44^{+0.03}_{-0.03}$	$14.45^{+0.02}_{-0.02}$	-1143 ± 6
C IV1549	1567.7329	50 ± 6	204 ± 5	$13.94^{+0.02}_{-0.03}$	$14.01^{+0.06}_{-0.07}$	-1147 ± 5
C IV1551	1570.3602	47 ± 5	156 ± 4	$14.04^{+0.02}_{-0.02}$	$14.33^{+0.05}_{-0.06}$	-1143 ± 5
System 2						
$\text{Ly}\alpha$	1234.4395	50 ± 8	16 ± 3	$12.48^{+0.07}_{-0.08}$	$12.63^{+0.08}_{-0.10}$	-303 ± 6
N V1239	1257.9923	90 ± 20	23 ± 5	$13.07^{+0.09}_{-0.11}$	$13.18^{+0.11}_{-0.14}$	-290 ± 6
N V1243	1262.0425	100 ± 50	10 ± 4	$13.00^{+0.15}_{-0.21}$	$12.99^{+0.25}_{-0.63}$	-289 ± 6
C IV1548	1572.1322	43 ± 10	42 ± 4	$13.03^{+0.04}_{-0.04}$	$13.23^{+0.10}_{-0.13}$	-295 ± 5
C IV1551	1574.7397	38 ± 10	29 ± 2	$13.16^{+0.03}_{-0.03}$	$13.44^{+0.11}_{-0.14}$	-296 ± 5

^aDerived from curve of growth arguments

^bDerived from optical depth integration

Table 4. Galactic and Unidentified Absorption Lines

λ_{Obs} [Å]	Ion	λ_{Rest} [Å]	FWHM [km s ⁻¹]	Equivalent Width [mÅ]	log(Column) [cm ⁻²] ^a	log(Column) [cm ⁻²] ^b	Velocity [km s ⁻¹]
1199.5251	N I	1199.550	76 ± 7	210 ± 10	14.50 ^{+0.46} _{-0.34}	14.25 ^{+0.06} _{-0.07}	-6 ± 7
1200.1924	N I	1200.223	65 ± 5	160 ± 10	14.41 ^{+0.36} _{-0.35}	14.30 ^{+0.05} _{-0.06}	-8 ± 7
1200.6842	N I	1200.710	90 ± 20	170 ± 10	14.76 ^{+0.40} _{-0.36}	14.50 ^{+0.05} _{-0.06}	-6 ± 7
1206.4296	Si III	1206.500	140 ± 10	500 ± 20	13.53-16.72	13.63 ^{+0.03} _{-0.03}	-18 ± 7
1224.3067 ^c	...		88 ± 4	251 ± 9			
1227.6204 ^c	...		122 ± 10	175 ± 7			
1235.6051	...		82 ± 9	42 ± 3			
1250.6094	S II	1250.584	60 ± 6	93 ± 8	15.15 ^{+0.04} _{-0.04}	15.18 ^{+0.05} _{-0.05}	+6 ± 6
1253.8245	S II	1253.811	60 ± 5	129 ± 7	15.05 ^{+0.03} _{-0.03}	15.09 ^{+0.03} _{-0.04}	+3 ± 6
1259.5310	S II	1259.519	64 ± 5	169 ± 5	15.10 ^{+0.02} _{-0.02}	15.13 ^{+0.02} _{-0.03}	+3 ± 6
1260.4310	Si II	1260.422	125 ± 3	498 ± 8	13.74-16.62	13.24 ^{+0.02} _{-0.02}	+2 ± 6
1263.5315	...		49 ± 9	33 ± 6			
1303.0942 ^d	O I	1302.168	883 ± 7	553 ± 5	15.04-18.45	14.80 ^{+0.08} _{-0.09}	+210 ± 70
1334.9145 ^d	C II	1334.532	560 ± 10	720 ± 30	14.82-20.81	14.18 ^{+0.21} _{-0.42}	+90 ± 70
1527.0709 ^d	Si II	1526.707	380 ± 60	280 ± 50	14.09-14.50	14.09 ^{+0.08} _{-0.10}	+70 ± 60
1548.1517	C IV	1548.187	97 ± 8	240 ± 20	13.83 ^{+0.04} _{-0.05}	13.79 ^{+0.09} _{-0.11}	-7 ± 5
1550.6375	C IV	1550.772	50 ± 10	120 ± 20	13.80 ^{+0.05} _{-0.06}	13.76 ^{+0.08} _{-0.10}	-26 ± 5

^aDerived from curve of growth arguments

^bDerived from optical depth integration

^cPossible Ly α forest lines. See Table 5.

^dFrom the low-resolution spectrum. The unusually large FWHMs indicate that these values should be used with caution.

Table 5. Likely Ly α Forest Lines

λ_{Obs} [Å]	FWHM [km s ⁻¹]	Equivalent Width [mÅ]	log(Column) [cm ⁻²] ^a	log(Column) [cm ⁻²] ^b	Rest Frame Velocity [km s ⁻¹]	Mrk 1044 Velocity [km s ⁻¹]
1224.3067	88 ± 4	251 ± 9	14.27 ^{+0.07} _{-0.07}	13.80 ^{+0.02} _{-0.03}	2130 ± 7	-2801 ± 7
1227.6204	120 ± 10	175 ± 7	13.79 ^{+0.04} _{-0.04}	13.56 ^{+0.05} _{-0.06}	2937 ± 7	-1994 ± 7
1228.3089	70 ± 20	45 ± 15	12.96 ^{+0.14} _{-0.19}	12.77 ^{+0.10} _{-0.13}	3117 ± 7	-1814 ± 7

^aDerived from curve of growth arguments

^bDerived from optical depth integration

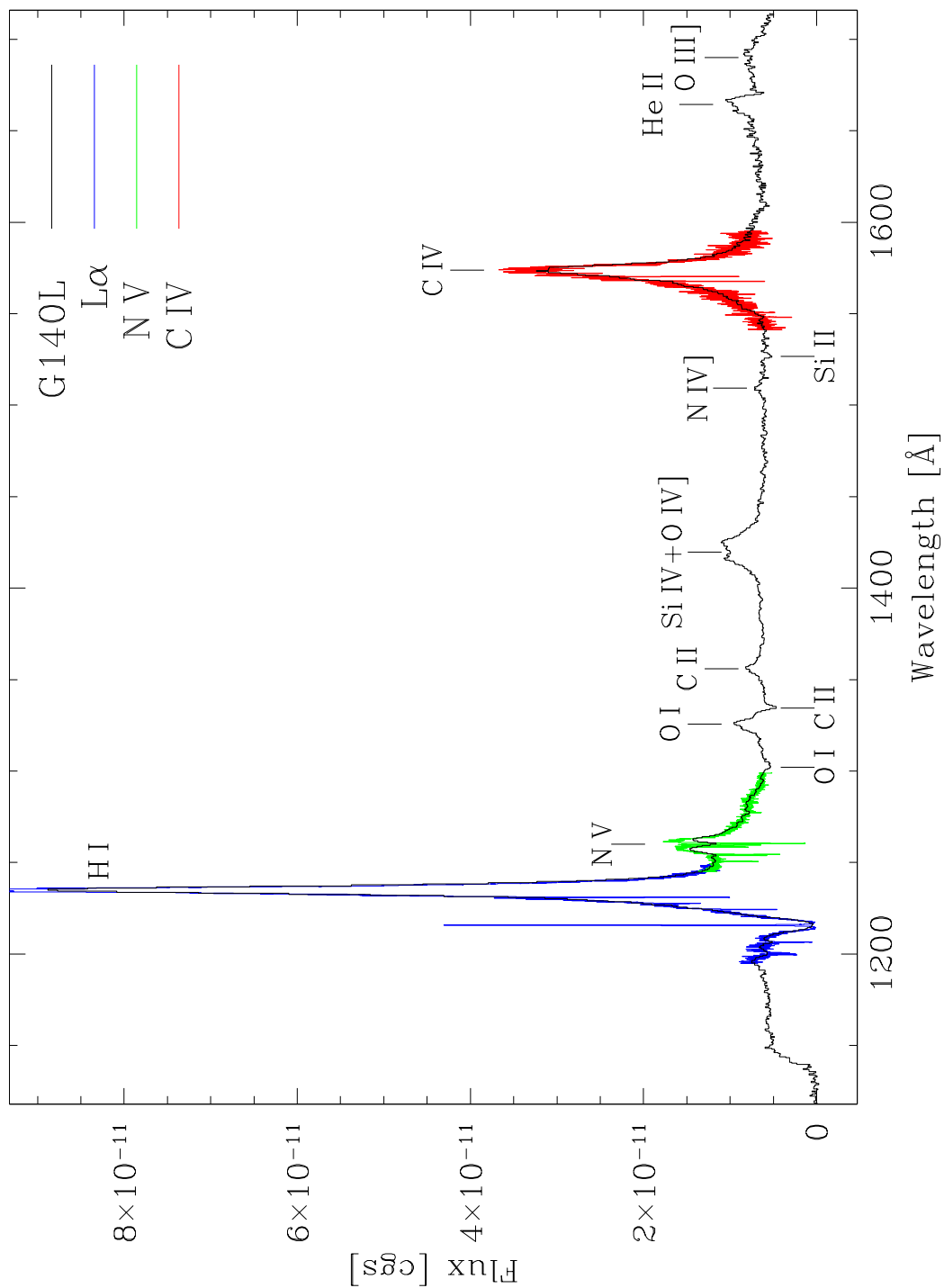


Fig. 1.— The three G140M spectra superposed over the G140L spectrum. The necessity of obtaining high-resolution spectra to determine the metallicity can be seen very well here. The C IV features are completely wiped out in the G140L spectrum. The N V feature visible in the G140L spectrum is, after consulting the G140M spectrum, seen mostly to be caused by Galactic absorption. The emission lines originating from Mrk 1044 are marked above the spectrum. The absorption lines caused by Galactic ISM are marked below the spectrum.

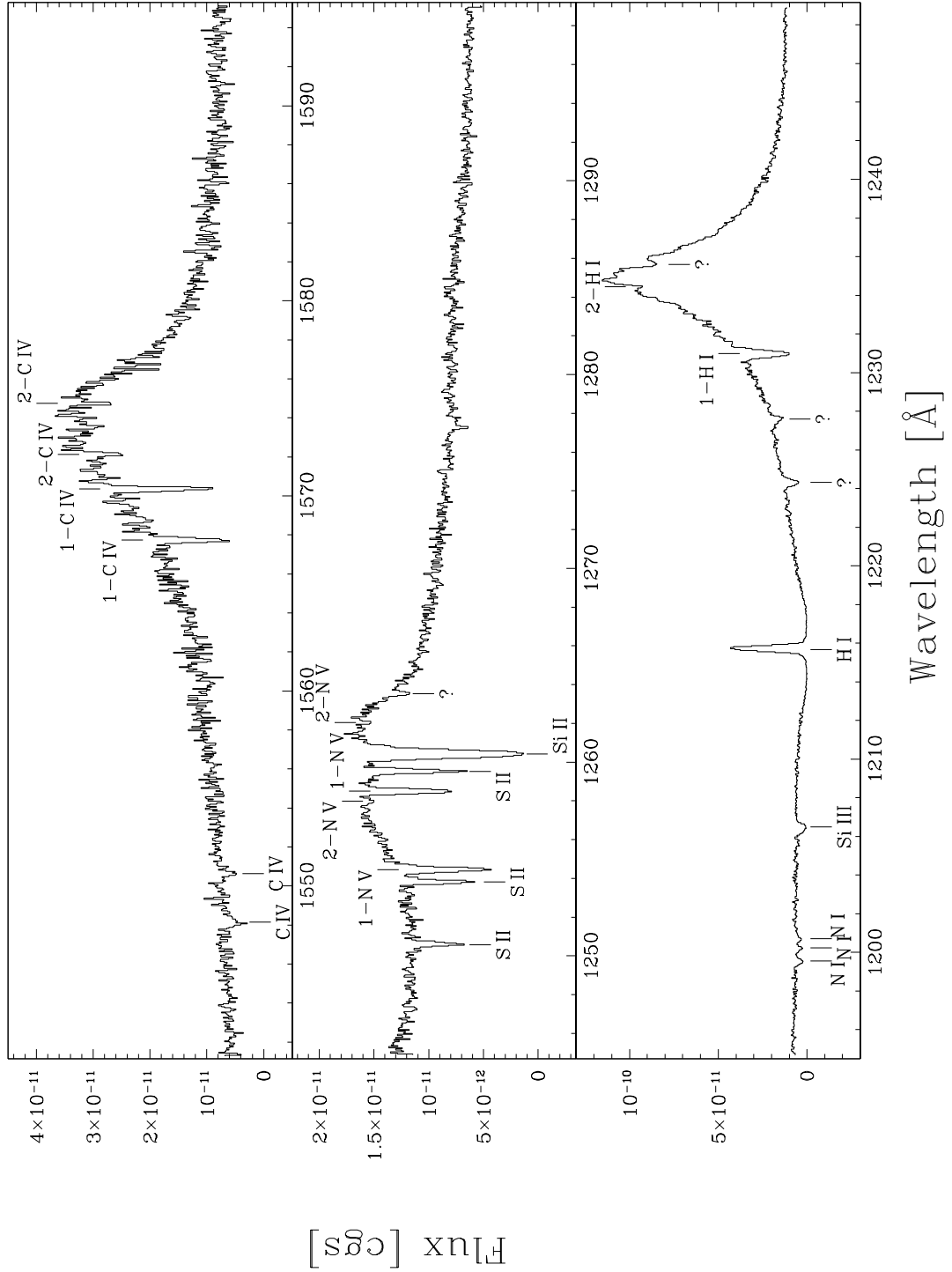


Fig. 2.— The three G140M spectra each shown separately. The absorption systems intrinsic to Mrk 1044 are marked above the spectrum and the identified Galactic lines are marked below the spectrum. Unidentified lines are marked as such.

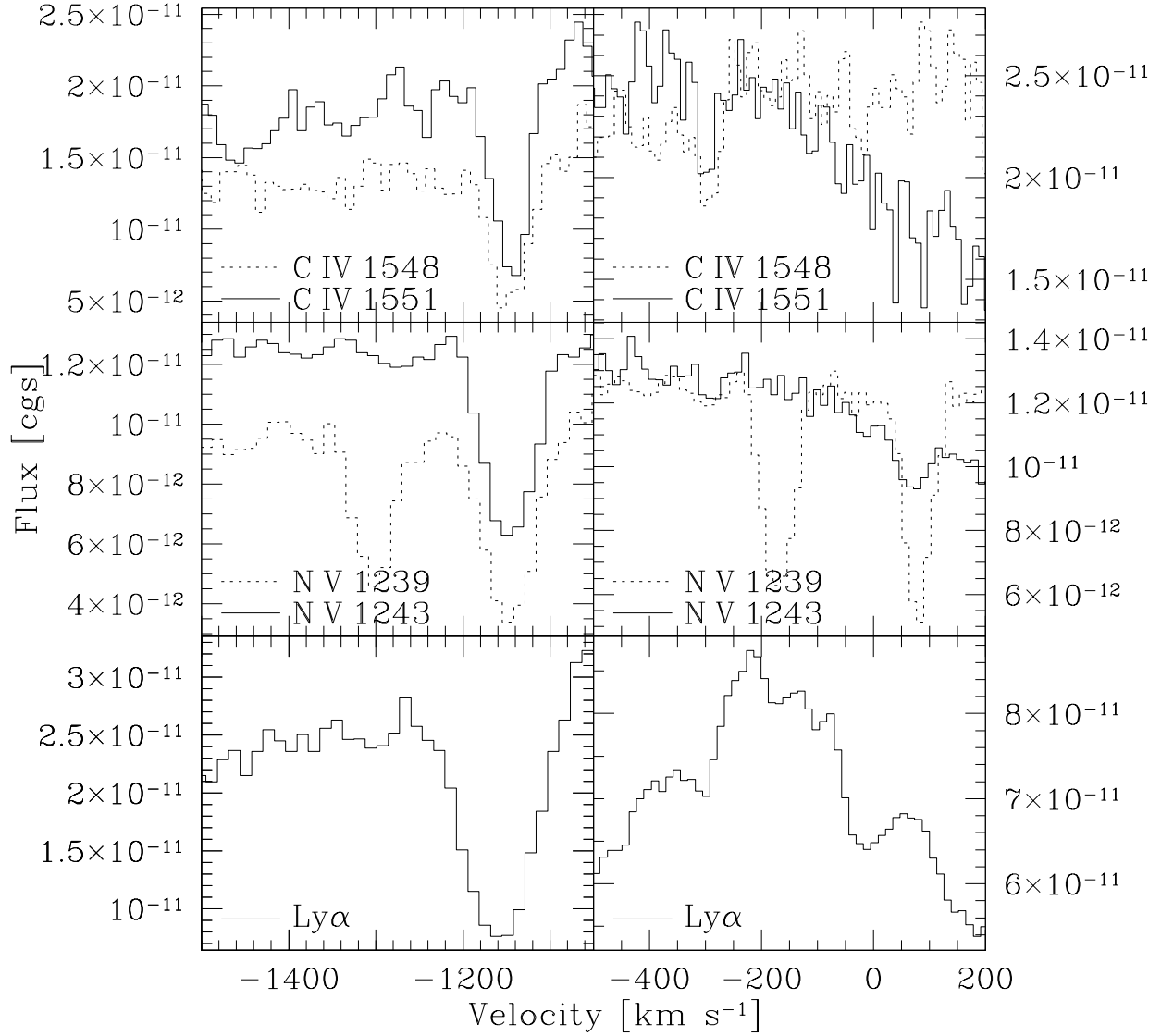


Fig. 3.— Velocity maps around Systems 1 (left) and 2 (right). In the case of C IV and N V, the dotted lines signify the shorter wavelength line of the pair, while the solid lines signify the longer wavelength line. System 1 is very secure with all three ions showing absorption at that velocity. System 2 is less obvious with the N V lines showing little contrast. Also visible at $\sim +75 \text{ km s}^{-1}$ is the chance alignment of a Galactic S II line with a yet unidentified line. Evidence against this candidate being a true system is the lack of corroborating absorption at that velocity in C IV and Ly α .

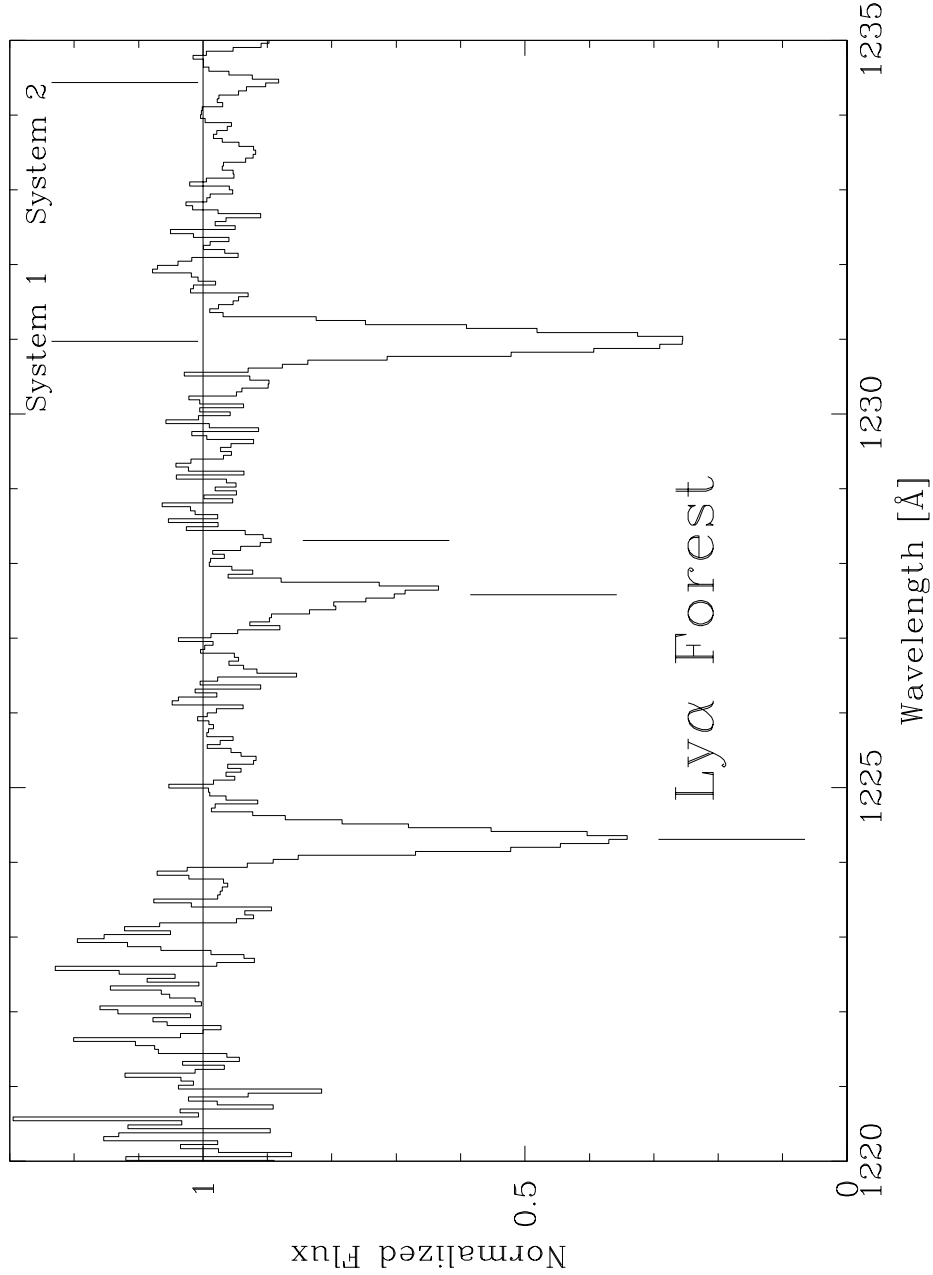


Fig. 4.— The normalized (continuum divided) spectrum blueward of the Ly α emission line of Mrk 1044. This is one of nine by-eye spline fits to the local continuum (i.e. the Ly α emission line) as described in §3. The absorption feature at 1228.3Å is a 3σ detection. Other possible absorption features such as those blueward of 1224Å or at 1233.5Å have significant detections in only some of the nine continuum fits. For example, the absorption feature at 1233.5Å is located near the steepest part of the Ly α emission line. Small changes in the perceived “continuum” level severely affect its properties. This also affects the absorption feature of System 2 to a lesser extent, though System 2 has the advantage of being confirmed by the presence of N V and C IV at the same velocity (see Figure 3).